



Tuning electronic structure of ZnO nanowires via 3d transition metal dopants for improved photo-electrochemical water splitting: An *ab initio* study

K.K. Korir^{a,*}, E.M. Benecha^b, F.O. Nyamwala^a, E.B. Lombardi^b

^a Mathematics and Physics Department, Moi University, P.O. Box 3900-30100, Eldoret, Kenya

^b College of Science, Engineering and Technology, University of South Africa, P.O. Box 392, UNISA, South Africa

ARTICLE INFO

Keywords:

ZnO nanowires
Photo-electrochemical
Water splitting
Density Functional Theory
Transition metals

ABSTRACT

ZnO nanowires have been proposed as potential photo-anode materials for photo-electrochemical water splitting due to their low toxicity, simple synthesis and easy modification routes. However, ZnO suffers from low PEC activity and photo-corrosion effects, and therefore, application of ZnO nanowires in PEC water splitting still awaits development of effective design and synthesis strategies to improve its PEC efficiencies to commercially viable levels. Here, we present *ab initio* Density Functional Theory calculations considering 3d transition metal doping as a potential route towards attainment of ZnO nanowires with superior PEC activity. Our results show that the stability of 3d transition metal dopants in ZnO NWs is dependent on the *d* character of the transition metal dopant as well as their concentration and doping site, with most transition metal atoms being energetically most favorable at the Zn substitutional site both in O-rich and Zn-rich conditions considered. Specifically, we find all 3d transition metal dopants in ZnO NW under O-rich conditions as well as Sc, Ti and V under Zn-rich conditions have negative formation energies at the considered dopant concentrations of 1–6 at. %, indicating that these dopants can readily be incorporated into ZnO NWs at thermodynamic equilibrium conditions. The electronic properties of Ti and V at 2% and 4% dopant concentration, respectively, yield a staggered band-structure configuration, while Sc, Cr, Mn, Co, Ni, and Cu dopants in ZnO NWs induce band-edge states. In addition, 3d TM dopants induces significant red-shift of the absorption edge of ZnO NW due to reduction in band gap, and are projected to improve visual light harvesting capabilities. Finally, the band alignment relative to the redox potential of water revealed that the valence band maximum of Sc, V, Ni and Cu doped ZnO NWs remains strongly positive above the oxidation potential of O₂/H₂O, while their reduction potential remain negative below the reduction potential of H⁺/H₂, favouring PEC applications.

1. Introduction

Over the last century, intensive use of carbon based energy sources has led to increase in atmospheric carbon dioxide (CO₂) gas concentrations that has induced anthropogenic climate change [1], whose adverse effects on the planet are being felt and projected to worsen, unless drastic CO₂ cuts are implemented as proposed in Kyoto protocol [2]. Development of alternative sources of energy with zero carbon footprint is therefore deemed critical for the survival of the planet. In this perspective, hydrogen fuel is one of the few clean energy sources that is considered a potential alternative to current carbon based fuels due to ready availability of the raw materials, relative ease of transportation

and storage, and high energy density [3,4]. In addition, hydrogen is an important feedstock in Fischer-Tropsch conversion of biomass-derived CO to a wide range of renewable hydrocarbons biofuels [5].

Currently, fossil fuels are the dominant source of industrial hydrogen, thus there is need for environmentally friendly sources of hydrogen. Water splitting has been identified as an elegant route towards sustainable production of hydrogen, in particular, since water is the key raw material and is available in large quantities in most parts of the world, thus making this approach quite attractive. Photo-electrochemical catalysis and electro-catalysis are some of the approaches of hydrogen fuel production via water splitting [6,7]. Photo-electrochemical (PEC) water splitting based devices utilize an

* Corresponding author.

E-mail address: kiptiemoikorir@mu.ac.ke (K.K. Korir).

<https://doi.org/10.1016/j.mtcomm.2020.101929>

Received 28 November 2020; Accepted 30 November 2020

Available online 2 December 2020

2352-4928/© 2020 Elsevier Ltd. All rights reserved.

active semiconductor anode material such as TiO_2 to absorb solar energy necessary to break the chemical bond of a water molecule [8–11].

Water splitting consists of two chemical reactions: the oxygen evolution reaction (OER) and hydrogen evolution reaction (HER). These processes are not thermodynamically favorable, hence require an external potential bias to drive the uphill reaction ($\Delta E^0 = -1.23$ V). The OER in an electrolytic cell is a four-electron transfer process (Eq. 1), and is considered the bottleneck in the decomposition of water molecule to form H_2 and O_2 gases.



Current industrial electrolyzers rely on external power sources to provide the required over-potential for water-splitting. However, integrating renewable energy sources such as solar energy with such electrolyzers is a more sustainable approach of hydrogen production. For example, using TiO_2 single crystal electrode, Honda et al. [11] were the first to demonstrate photon driven water oxidation, and since then, huge efforts have been directed towards understanding the various processes involved, with the aim of optimization of such processes. Notwithstanding earlier successes in the demonstration of PEC water splitting using TiO_2 , little has been attained in improving light conversion efficiencies, and has mainly attributed to TiO_2 activation energy being limited to the UV spectral region. On this basis, development of other photo-catalysts adept for efficient photo-induced charge separation is emerging as an important research area. In this regard, zinc oxide (ZnO) has emerged as a potential photo-anode material due to its low toxicity, availability in various nanostructure configurations, and well established synthesis and modification routes [12–14]. Furthermore, in semiconductor nanocrystals such as nanowires, quantum confinement can be leveraged to attain superior optical properties via manipulation of electron-hole interaction due to size dependence [15,16]. However, practical applications of ZnO nanostructures for PEC water splitting still awaits development of better design and synthesis strategies that can push their efficiency to commercially viable levels.

Tuning the electronic structure of ZnO nanostructures in order to enable it to function in the visible portion of the spectrum (rather than only under UV illumination), by using doping or surface functionalization with photosensitizers, has been identified as a promising route towards achievement of superior PEC water splitting efficiencies [17–19]. In addition, doping ZnO nanowires with transition metals (TM) has been shown to improve charge separation, while reducing its band gap and photo-corrosion effect, thus improving its performance in PEC applications. For example, Cu doping has been shown to reduce the optical band gap of ZnO nanorods [20], thus extending the optical absorption edges with an overall effect of dramatically improving photosensitivity to both UV and visible light [21,22]. In the case of Vanadium doped ZnO nanorods, high photocurrent densities of up to 4 orders of magnitude higher compared to that of pristine ZnO nanorods [23], while Mn^{2+} doped ZnO nanofibers have been shown to exhibit excellent visible light photo-catalytic activity (with a quantum efficiency of up to 13 %) and reduced photo-corrosion [24]. Yet to the best of our knowledge, comprehensive studies that considers a wider range of transition metals as potential dopants for adapting ZnO nanowires for enhanced PEC water splitting is lacking. The few fragmented studies that exist may not be sufficient to determine ideal dopants for the development of superior ZnO photo-catalyst. Therefore, in the current work, we apply Density Functional Theory calculations (DFT) to systematically investigate trends in chemical stability and electronic properties of 3d transition metal doped ZnO NWs. In particular, we identify potential dopants, optimal concentration, and stability, which may be of relevance in the

synthesis of such systems.¹

2. Computational details

Spin-polarized calculations were carried out within the framework of DFT, as implemented in the Quantum Espresso suite [25]. The generalized gradient approximation to the exchange and correlation functional was employed in the form proposed by Perdew, Burke and Ernzerhof (PBE) [26]. The core-electrons were replaced with ultra-soft pseudo-potentials following Vanderbilt's formulation [27], and the electronic wave functions and charge densities were expanded in a plane wave basis set with a converged energy cutoff ; of 28 Ry and 280 Ry, respectively.

ZnO NWs were modeled as rods along the z-axis, corresponding to the wire axis, with the non-polar surface [1100] being the dominant surfaces along the length of the nano-rods. All the calculations reported this work considered a supercell consisting of one ZnO NW unit cell of 2.3 nm in diameter, with 48 Zn atoms and 48 O atoms, with vacuum of 15 Å (along the x and y axes) to avoid interaction between periodic images. A well converged Monkhorst pack grid of $1 \times 1 \times 8$ was used for integration over the Brillouin zone [28]. In all cases the geometry optimizations were performed using the conjugate gradient algorithm until all residual forces were smaller than 0.02 eV/Å. The total energy for ionic minimization was considered converged once the total energy changes less than 10^{-8} eV between two consecutive SCF steps and the full geometry optimization without any symmetry restrictions was performed. In addition, ZnO NWs of sizes ranging from 0.5 nm to 2.3 nm were used to investigate the size effect on the electronic band-gap.

DFT to ZnO is known to produce severe underestimation of the electronic band gap in ZnO due to unphysical interaction between the Zn d-band and the O p-band. Here, we employed the DFT+U scheme to properly compute the electronic properties of the structures relaxed at the PBE level, with $U = 12.0$ eV and $U = 6.5$ eV for the Zn 3d orbitals and O 2p orbitals, respectively. These values have been shown to effectively correct DFT band-gap underestimation for ZnO [29,30]. The U values of 3d TM dopants considered in this work were obtained from literature [31–34].

3. Results and discussion

3.1. Stability trends of 3d transition metals dopants in ZnO NWs

Transition metal defects are known to modify the electrical and optical properties of semiconductors, and thus can be used judiciously to modify the properties of semiconductor hosts for target applications. Indeed, point defects such as substitutional defects tend to occur randomly in a periodic crystal depending on the growth technique [35–37]. In this work, substitutional and interstitial sites were considered at the surface and near surface of the respective ZnO nanowires as shown in Fig. 1, since a catalytic reaction occurs at the surface of the nanowire.

Understanding the incorporation, stability and behavior of such defects in ZnO NWs is therefore essential to its successful application in PEC water splitting. Formation energies for the various defects were determined using Eq. 2 below,

$$E_{FM} = E_{NWS}(\text{ZnO} : M) - E_{NWS}(\text{ZnO}) + (\mu_{\text{Zn/O}} - \mu_M), \quad (2)$$

where $E_{NWS}(\text{ZnO} : M)$ is the total energy of the doped NW, $E_{NWS}(\text{ZnO})$ is the total energy of undoped NW, $\mu_{\text{Zn/O}}$ is the chemical potential of the

¹ Doping can lead to defects that can act as recombination centers, thus reducing the efficiency of the photo-catalysts regardless of the visible light absorption capabilities, therefore comprehensive understanding is needed before such procedures are deemed viable.

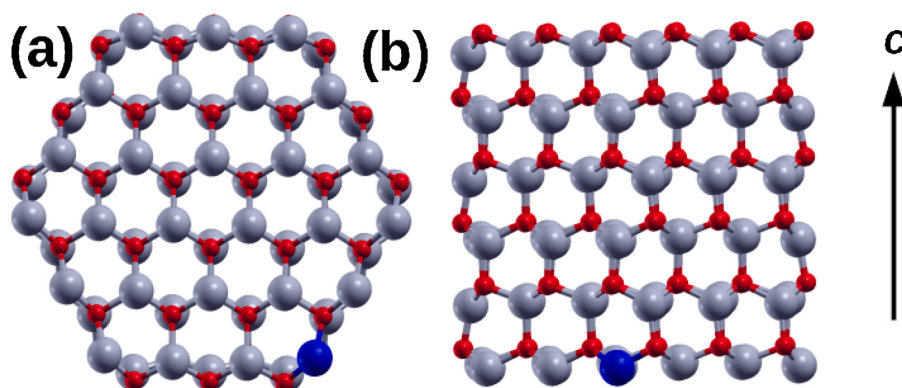


Fig. 1. (a) Top view, and (b) side view of ZnO NW with 2.3 nm diameter. In panel (b) three unit cells along [0001] axis of the NW axis was utilized. Grey (red) spheres represent zinc (oxygen) atoms while blue spheres represent TM substitutional dopants. (For interpretation of the references to colour in this figure legend, the reader is referred to the web version of this article).

substituted zinc/oxygen atoms, and μ_M is the chemical potential of the 3d metal dopant atoms. The formation energies of 3d transition metal atoms in ZnO NW were calculated at the Zn substitutional, O substitutional and interstitial sites both under O-rich and Zn-rich growth conditions [38]. Under the O-rich limit, $\mu_O^{\max} = \frac{1}{2}E(O_2)$ and $\mu_{Zn}^{\min} = E(ZnO) - \mu_O^{\max}$, while under the Zn-rich limit, $\mu_{Zn}^{\max} = E(Zn)$ and $\mu_O^{\min} = E(ZnO) - \mu_{Zn}^{\max}$, where $E(O_2)$, $E(Zn)$ and $E(ZnO)$ are the calculated total energies of the oxygen molecule, pure crystalline Zn and ZnO unit cells, respectively. Similarly, the chemical potentials of the transition metal dopants, were determined from their respective pure crystalline phases.

We find the formation energies of transition metal dopants in ZnO NWs to be strongly dependent on the doping site and the d character of the transition metal atom, as shown in Fig. 2, consistent with trends observed in bulk ZnO [39]. The formation energy increases from Sc to Cu under both the O-rich and Zn-rich conditions for both Zn and O sites, a trend which can be explained in terms of the decreasing number of valence electrons in the d orbital across the 3d elements.

Under O-rich conditions, all TMs considered are energetically stable on Zn site, with negative formation energies (ranging from -0.8 eV to -6.2 eV) as shown in Fig. 2 (a). While interstitial and O substitutional sites are energetically less favorable under O-rich conditions. Under Zn-rich conditions, shown in Fig. 2(b), we find a similar trend in the magnitude of formation energy for the Zn-substitutional, O-substitutional and interstitial doping. However, for smaller atomic radii transition metal atoms (Fe, Co, Ni and Cu), the formation energy difference between various doping sites is close (less than 0.5 eV), indicating that the interstitial and substitutional defects may co-exist in ZnO NWs in as-grown samples in Zn-rich conditions. Indeed, interstitial 3d metals dopants in ZnO NWs have been shown to increase electrical conductivity by inducing p -type semi-conducting character, while enhancing optical

transmittance at higher concentration [40].

Additionally, we find that the oxygen substitutional site under O-rich conditions is much higher in energy compared to the Zn substitutional site, as shown in Fig. 2(a). This observation can be attributed to large crystal strain due to relatively large atomic radii of TM atoms compared to O atoms. Importantly, our calculated formation energies of all 3d the transition metals in ZnO NW at the Zn substitutional site in the O-rich condition are negative. Similarly, the formation energies of Sc, Ti and V at the Zn substitutional site in the Zn-rich condition are also negative. The negative formation energies indicates that these transition metals can readily be incorporated into ZnO NWs at the Zn substitutional site under equilibrium conditions. Moreover, many experimental data indicate that the growth of ZnO often occur through non-equilibrium processes [41,42], therefore, techniques such as ion implantation, may also be used to achieve transition metal doping with positive formation energies, albeit at relatively lower concentrations.

To investigate the influence of transition metal dopants on the electronic and optical properties of ZnO NWs for PEC applications, we first investigate their stability as a function of dopant concentration by increasing the number of TM dopants randomly distributed in the NW at substitutional Zn sites. The same doping position was maintained for each respective transition metal atom at all doping concentrations considered in this study.

Fig. 3 illustrates trends in the formation energies of 3d TM dopants in ZnO NW for various dopant concentrations (1, 2, 4 and 6 at. %) under O-rich and Zn-rich conditions. It is observed that the formation energy of 3d TM atoms in ZnO NW is sensitive to dopant concentration. For example, under O-rich conditions, the stability of transition metal doped ZnO NW increases with an increase in dopant concentration. Interestingly, in Zn-rich conditions, this trend is reversed for transition metals in the middle (Cr, Mn, Fe) or late (Co, Ni, Cu) 3d series, with the defect

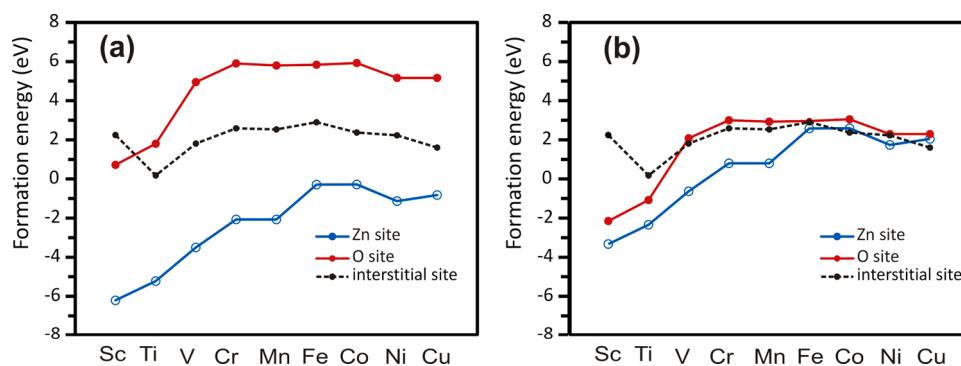


Fig. 2. Formation energy profile of 3d transition metal defects in ZnO NW calculated for Zn substitutional, O substitutional and interstitial defect site in (a) O-rich and (b) Zn-rich conditions.

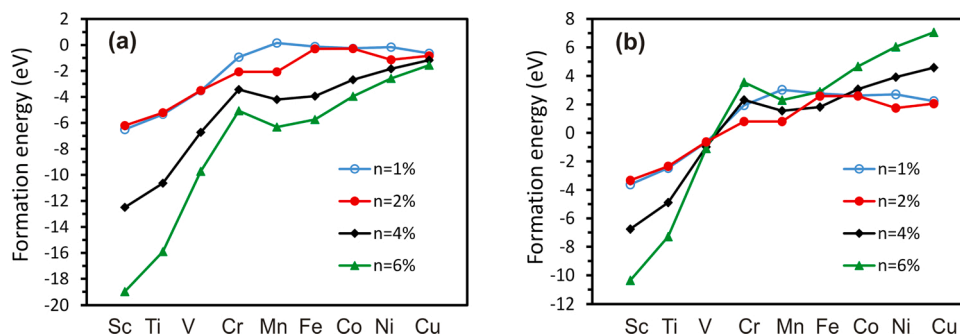


Fig. 3. Formation energies of 3d TM dopants as a function of dopant concentration (1-6 atm. %) at Zn substitutional sites under O-rich and Zn-rich conditions.

stability decreasing with increasing in dopant concentration, consistent with experimental studies that have shown Fe concentrations higher than 5 atm. % induces dramatic changes in the structural morphology of the NW [43]. These observations may be attributed in part to lower atomic radii of these elements compared to that of Zn, thus subjecting the ZnO crystal to substantial local structural relaxation. Also, elements in the middle and late 3d series have fewer unoccupied *d* orbitals hence affect the level of their chemical interaction with nearest neighbor oxygen atoms.

Under both O-rich and Zn-rich conditions, we find that the defect stability remains insensitive to changes in dopant concentration of 1–2 at m. %. Beyond this concentration, stability to increase/decrease as discussed above. Moreover, under O-rich conditions, the change in stability of transition metal doped ZnO NW with dopant concentration is minimal in late 3d transition metal atom doping, with Cu-doped ZnO being the least sensitive to changes in dopant concentration. On the other hand, in the Zn-rich limit, the change in stability is minimal in the middle of the 3d series, with V-doped ZnO NW being the least sensitive to changes in dopant concentration. Since PEC water splitting is a carrier controlled process, our work presents an important finding that may guide fabrication of TM-doped ZnO NWs for practical PEC applications, in particular, it is observed that dopant species and concentration tend to moderate electron carrier in ZnO NW.

3.2. Effects of 3d transition metal dopants on electronic properties of ZnO NWs

In low-dimensional systems such as ZnO NWs, band-gap broadening occurs due to quantum confinement and large surface area to volume ratio effects; overlapping energies that are usually observed in bulk systems tend to spread out, becoming more quantized, thus widening the

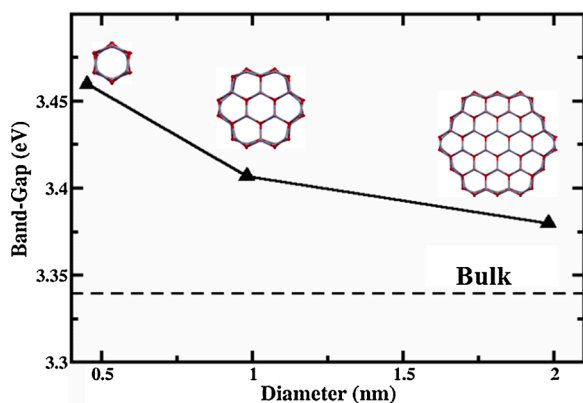


Fig. 4. Bandgap of ZnO NWs of various diameters compared to that of bulk ZnO. Ball and stick representation of ZnO, where red and grey balls represent Zn and O atoms, respectively. (For interpretation of the references to colour in this figure legend, the reader is referred to the web version of this article).

band gap, as shown in Fig. 4. For PEC water splitting, a reduced band-gap in ZnO NWs is desirable as it would enable harvesting solar energy from both the visible and near-infrared parts of the spectrum. Therefore, band-gap engineering in ZnO NWS is necessary for increased efficiency, as proposed in the current work via 3d TM doping.

We find that most 3d TM doped ZnO NWs have reduced band-gaps compared to pristine NWs, which can be attributed to the downward shift in conduction band minimum and an upward shift in valence band maximum, consistent with previous studies [44–46].

Fig. 5 summarizes the band gap energy of transition metal doped ZnO NW at the Zn substitutional as a function of dopant concentration. We observe that the band gap of transition metal doped ZnO NWs is strongly dependent on the dopant concentration. In general, we find that doping leads to an overall reduction in the ZnO NW band gap due to shifting of the band edge levels. In Ti, V, Mn and Fe doped ZnO NW, a drastic band gap reduction is observed with increase in dopant concentration from 1 to 6%, shifting optical response towards the visible light spectrum at higher dopant concentrations. In the case of Mn, the band gap becomes zero at 6 atm. %, making the system metallic due to upward shift of the Fermi level, as shown in Fig. 5(b). The observed reduction in band-gap in these cases can be attributed to upward shift of the valence band maximum (VBM) and downward shift of conduction band minimum (CBM) due to the introduction of defect states, consistent with experimental work [31,47]. Since PEC applications require the NW to retain a semiconducting character (for electron-hole separation to facilitate the redox reaction), dopant concentrations in Mn-doped ZnO NW must therefore remain at sufficiently low levels to prevent semiconductor-metal transition.

In the case of Cr, Co, Ni and Cu doping, an increase in the dosage concentration results in the broadening of the ZnO NW band gap. This effect can be attributed to the downward shift of the valence band maximum (VBM). In Ti, V, Mn and Fe doped ZnO NW, a drastic band gap narrowing is observed with increase in dopant concentration from 1 to 6%, while in the case of Sc doping, a further increase in the concentration dosage has a negligible effect on the magnitude of the band gap.

An occurrence of mid-gap states between VBM and CBM and can extend the absorption spectral range of wide band-gap semi-conductors from UV to visible light range. Furthermore, shallow mid-gap states can influence holes transfer in water oxidation by bringing the catalyst level close to the H₂O/O₂ redox level [48]. We find that ZnO NWs doped with Ti and V at 4% and 2% defect concentration, respectively, induce mid-gap states, which can be attributed to hybridization of O-2*p* and V/Ti-3*d* orbitals, as shown in Fig. 6. In both Ti and V doping, the reduction of band-gap can be attributed to the formation of impurity states near the bottom of CBM of ZnO NW that merge with conduction band, as shown in Fig. 6(c–d).

Therefore, with appropriate dopant dosage, both Ti and V can yield a staggered band-structure configuration, which is ideal for PEC and related applications

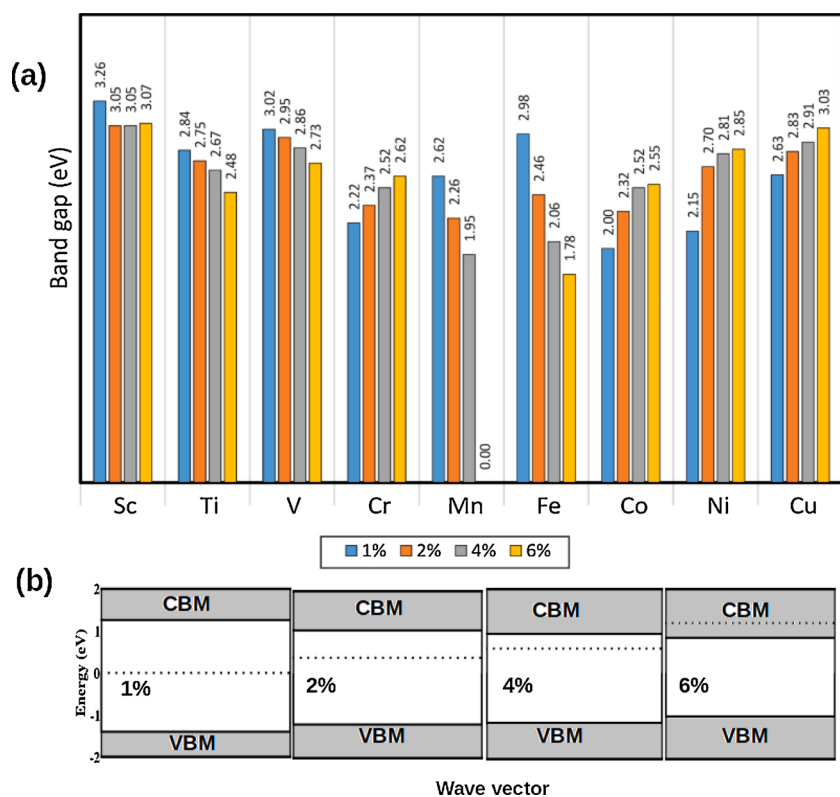


Fig. 5. (a) Band-gap energy of ZnO NWs doped with 3d TM metals at the Zn substitutional site, with dopant concentrations ranging from 1-6%. Doping leads to an overall reduction of the band gap relative to the band gap of undoped ZnO NW (3.37 eV). Figure (b) shows semi-conductor-to-metal transition in Mn doped ZnO NW that occurs at 6%, and attributed to upward shift of Fermi level and downward and upward shift of CBM, and VBM, respectively. The dotted line denotes the Fermi level.

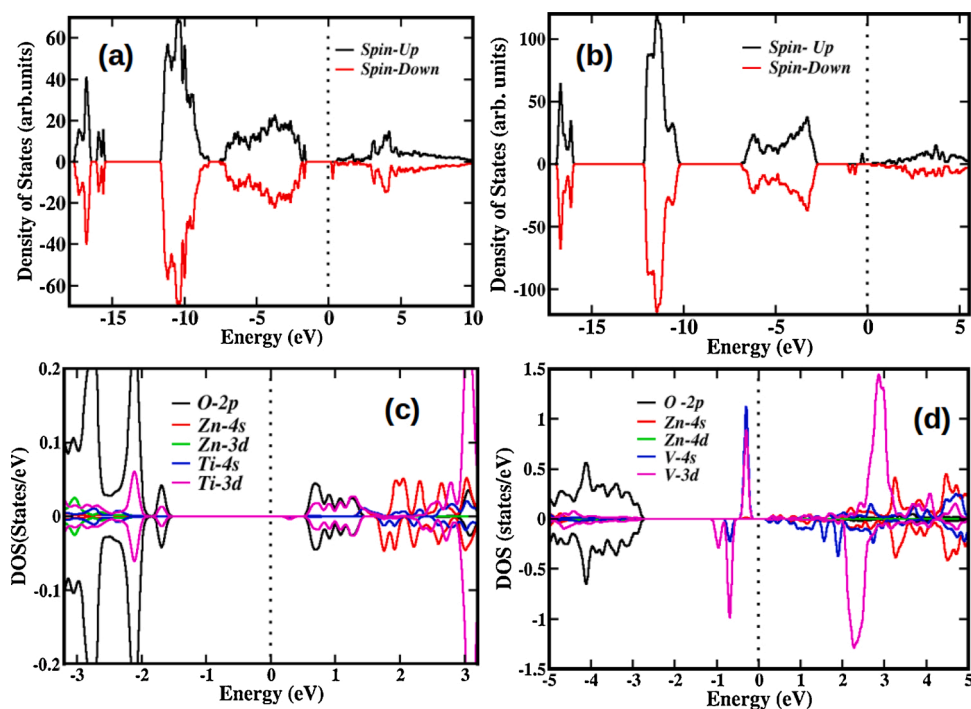


Fig. 6. Density of states of (a) ZnO NW doped with 4% Ti, and (b) ZnO NW doped with 2% V while the lower pane (c) and (d) shows the corresponding projected density of states, respectively. The Fermi level is indicated by the dotted line.

3.2.1. Optical response of Ti and v doped ZnO NWs

The effect of TM dopants on the optical properties of ZnO NWs is investigated via time dependent density functional perturbation theory (TDDPFT) using Liouville-Lanczos approach [49]. In order to evaluate the PEC performance of transition metal doped ZnO NWs, we consider their optical properties since NWs are anticipated to harvest solar energy

to drive PEC activity, thus should be able to have optimal harvesting capability and target electromagnetic spectrum with maximum energy

The dielectric response function is expressed as $\epsilon(\omega) = \epsilon_1(\omega) + i\epsilon_2(\omega)$, where ϵ_1 and ϵ_2 are the real and imaginary part of the dielectric function, respectively. The imaginary part of the dielectric function is obtained by summing all possible transitions from unoccupied to the

occupied wave-functions using dipole transition matrix, while the real part of the dielectric function is determined using the Kramers-Kronig relation. A more detailed description of optical properties calculations within context of TDDFT may be found in references [50,51]. The optical absorption coefficient (α_{abs}) is calculated from the dielectric response function [52] using Eq. 3, as shown,

$$\alpha_{abs} = \sqrt{2\omega} \left(\sqrt{\varepsilon_1^2(\omega) + \varepsilon_2^2(\omega)} - \varepsilon_1(\omega) \right)^{\frac{1}{2}}. \quad (3)$$

Both Ti and V dopants at 4% and 2% concentration, respectively, in ZnO NWs yielded a staggered band-structure configuration ideal for PEC activity, here, we perform optical characterization focusing on these dopants as a case study.

The calculated α_{abs} for pristine and doped (4% Ti and 2% V) ZnO NWs are presented in Fig. 7. Our results shows that the absorption spectrum of both pristine and doped ZnO NWs depends on the polarization of the incoming light, with parallel beams being more red-shifted compared to perpendicular beams, as shown in Fig. 7. The reference surface considered in this work is (1100) non-polar surface that is the dominant surface in ZnO NWs, thus is anticipated that PEC and other related activities would occur on this surface.

Further, a comparison of absorption spectrum of pristine ZnO NW to that Ti and V doped ZnO NW shows a significant red-shift of the band-edge, consistent with previous studies that have shown that doping with TM atoms introduces optically active sites that causes red-shift of the optical absorption [40,41]. On the basis of these results, it can be deduced that Ti and V dopants induces significant red-shift of the absorption edge of ZnO NW due to reduction in band gap, and are projected to have enhance PEC activity due to improved visible light harvesting capabilities

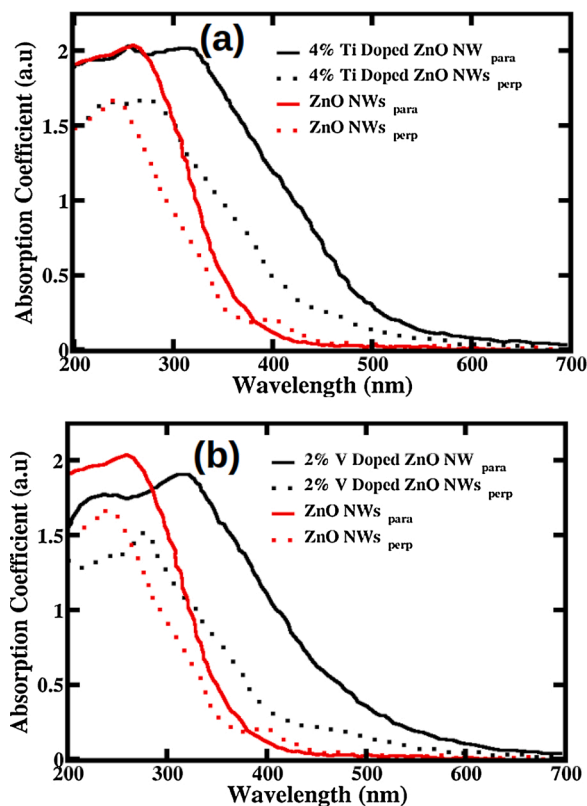


Fig. 7. Calculated optical absorption coefficients of (a) Ti doped ZnO NWs, and (b) V doped ZnO NWs with dopant concentration of 4% and 2 %, respectively). The parallel (para) and perpendicular (perp) direction of incoming light relative to the ZnO (1100) surface are considered in this work.

3.3. Photocatalytic activity

The generation, separation and transfer of photo-induced electron-hole pairs in PEC water splitting can be estimated by evaluating band alignment of the photocatalyst relative to the redox potential of water [53,54]. The conduction band minimum (CBM) and valence band maximum (VBM) potential on the normal hydrogen electrode (NHE) scale is calculated as [55–57].

$$E_{CB}^{NHE} = \chi - E_e - 0.5E_g \quad (4)$$

$$E_{VB}^{NHE} = E_{CB}^{NHE} + E_g$$

Where χ is the absolute electronegativity of the semiconductor, E_e is the energy of a free electron on the NHE scale (4.5 eV) and E_g is the band gap of the semiconductor.

To evaluate the effect of TM dopants on the photocatalytic performance of ZnO NWs, we plot the band edge alignment of pure and doped ZnO NW for different dopant concentrations compared with the reduction and oxidation potentials of water, as shown in Fig. 8. Photocatalytic water splitting can occur if the CBM of the photocatalyst is more negative relative to the redox potential of H^+/H_2O (0 V vs. NHE) while the VBM is more positive relative to the redox potential of O_2/H_2O (1.23 V) [54].

As shown in Fig. 8, the CBM of intrinsic ZnO NW is higher (by about 0.25 eV) than the reduction potential of H^+/H_2 , while the VBM is more positive (by 1.75 eV) than the oxidation potential of O_2/H_2O . This implies that pure ZnO NW has a good oxidation and reduction ability, however with a band gap of 3.4 eV, which requires UV light illumination. In order to enable water splitting at visible light frequencies, band gap engineering is required as shown in Section 3.2 above, and the ideal TM dopant is the one that narrows the band gap of the ZnO NWs while maintaining the semi-conductor character by shifting the CBM and VBM relative to pure ZnO NW, making it a candidate for visual light illumination rather than UV light. In addition to band gap engineering, levels of CBM/VBM relative to redox potentials of water need to be considered, as well as any defect levels in the band gap, as this factors have strong effect on overall PEC activity of the photocatalyst.

We find that the VBM of 3d TM doped ZnO NWs remains strongly positive above the oxidation potential of O_2/H_2O , favouring oxygen

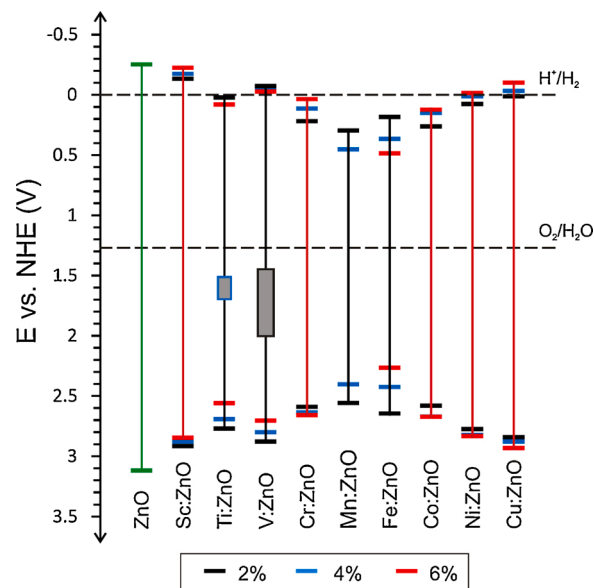


Fig. 8. Band edge alignment of the pure and 3d transition metal doped ZnO NW relative to the redox potential of water for different dopant concentrations (2%, 4%, 6%). The grey boxes in Ti and V doped ZnO NWs correspond to the impurity bands (See Fig. 6) at 4% and 2% dopant concentrations, respectively.

evolution for all 3d TM's. On the other hand, the reduction potential of Cr, Mn, and Co doped ZnO NW remains negative below the reduction potential of H^+/H_2 . Ti doped ZnO NW at 2% dopant concentration lies on reduction potential of H^+/H_2 while other dopant concentrations remain below reduction potential.

The reduction potential of Sc, V, Ni and Cu doped ZnO NWs are positive and above reduction potential of H^+/H_2 by 0.23 eV, 0.08 eV, 0.02 eV and 0.10 eV, respectively, depending on dopant concentration. This result makes ZnO NWs doped with Sc, V, Ni or Cu transition metals potential photocatalyst for simultaneous evolution of hydrogen and oxygen. Therefore, tuning the dopant concentration presents a possibility of improving the photocatalytic driving force.

4. Conclusion

In light of the previously demonstrated potential of ZnO NW's for PEC and related applications, we have systematically investigated the stability and electronic properties of 3d TM doped ZnO NWs by means of *ab initio* DFT simulations. Our results show that defect formation in ZnO NWs is strongly dependent on defect site and *d* character of transition metal dopant. The Zn substitutional site is the most energetically favorable for most 3d TM dopants in both Zn-rich and O-rich growth conditions. Under O-rich condition, all 3d transition metals at Zn-substitutional site as well as Sc, Ti and V under Zn-rich conditions have negative formation energy, indicating that they can be incorporated readily in ZnO NWs under equilibrium conditions. Further, the formation energy difference between the substitutional site and interstitial site for small atomic radii 3d TM dopants Fe, Co, Ni, and Cu is negligible in Zn-rich conditions, suggesting possible co-existence of these two defect configurations in ZnO NWs for these transition metal dopants. The stability of 3d transition metal atoms in ZnO NWs is also critically dependent on dopant concentration, with Sc, Ti and V being the most energetically favourable within the dopant concentration range of 1–6% considered in this study.

In addition, Ti and V induce significant red-shift of the absorption edge of ZnO NW due to reduction in band gap, and are projected to enhance PEC activity due to their enhanced visible light harvesting capabilities.

Further, band alignment relative to the redox potential of water revealed that the VBM of Sc, V, Ni and Cu doped ZnO NWs remains strongly positive above the oxidation potential of O_2/H_2O , favouring oxygen evolution, with the reduction potential remaining negative below the reduction potential of H^+/H_2 . In summary, we have explored the effect of 3d TM dopants on PEC activity ZnO NWs, taking into account formation energies, defect sites, concentration and defect levels in the band gap, and have predicted the suitable 3d TM's dopants for enhancing PEC water splitting efficiency of pristine ZnO NW's. Therefore, our findings will assist in identifying the appropriate dopants and concentration dosages in ZnO NW's, and will contribute to tuning properties of ZnO NWs for optimal PEC water splitting.

Authors contributions

K. K. Korir and E. M. Benecha: Performed the calculations, data analysis, and manuscript writing.

F. O. nyanwala and E. B. Lombardi: Performed data analysis and manuscript writing.

Declaration of Competing Interest

The authors report no declarations of interest.

Acknowledgements

The authors acknowledge funding from ACEII-PTRE of Moi University, and CHPC-Cape Town for the availability of High Performance

Computing resources and support. EMB acknowledges financial support from NRF-South Africa under grant number KIC180417321935.

References

- [1] T.A. Faunce, W. Lubitz, A.B. Rutherford, D. MacFarlane, G.F. Moore, P. Yang, et al., Energy and environment policy case for a global project on artificial photosynthesis, *Energy Environ. Sci.* 6 (3) (2013) 695–698.
- [2] Y. Li, J.Z. Zhang, Hydrogen generation from photoelectrochemical water splitting based on nanomaterials, *Laser Photon. Rev.* 4 (4) (2010) 517–528.
- [3] M. Balat, Potential importance of hydrogen as a future solution to environmental and transportation problems, *Int. J. Hydrogen Energy* 33 (15) (2008) 4013–4029.
- [4] T. Hisatomi, J. Kubota, K. Domen, Recent advances in semiconductors for photocatalytic and photoelectrochemical water splitting, *Chem. Soc. Rev.* 43 (22) (2014) 7520–7535.
- [5] W. Kreuter, H. Hofmann, Electrolysis: the important energy transformer in a world of sustainable energy, *Int. J. Hydrogen Energy* 23 (8) (1998) 661–666.
- [6] Z. Liu, Y. Jiang, X. Liu, G. Zeng, B. Shao, Y. Liu, et al., Silver chromate modified sulfur doped graphitic carbon nitride microrod composites with enhanced visible-light photoactivity towards organic pollutants degradation, *Compos. Part B: Eng.* 173 (2019), 106918.
- [7] Q. Liang, X. Liu, G. Zeng, Z. Liu, L. Tang, B. Shao, et al., Surfactant-assisted synthesis of photocatalysts: mechanism, synthesis, recent advances and environmental application, *Chem. Eng. J.* 372 (2019) 429–451.
- [8] A. Ursula, L.M. Gandia, P. Sanchis, Hydrogen production from water electrolysis: current status and future trends, *Proc. IEEE* 100 (2) (2011) 410–426.
- [9] C. Xiang, K.M. Papadantonakis, N.S. Lewis, Principles and implementations of electrolysis systems for water splitting, *Mater. Horiz.* 3 (3) (2016) 169–173.
- [10] K. Zeng, D. Zhang, Recent progress in alkaline water electrolysis for hydrogen production and applications, *Prog. Energy Combust. Sci.* 36 (3) (2010) 307–326.
- [11] A. Fujishima, K. Honda, Electrochemical photolysis of water at a semiconductor electrode, *Nature* 238 (5358) (1972) 37–38.
- [12] Ü. Özgür, Y.I. Alivov, C. Liu, A. Teke, M. Reschchikov, S. Dogan, et al., A comprehensive review of ZnO materials and devices, *J. Appl. Phys.* 98 (4) (2005) 11.
- [13] K.K. Korir, A. Catellani, G. Cicero, Tailoring oxygen vacancies at ZnO (1 1 - 00) surface: an ab initio study, *J. Appl. Phys.* 120 (12) (2016) 125301.
- [14] A. Wolcott, W.A. Smith, T.R. Kuykendall, Y. Zhao, J.Z. Zhang, Photoelectrochemical study of nanostructured ZnO thin films for hydrogen generation from water splitting, *Adv. Funct. Mater.* 19 (12) (2009) 1849–1856.
- [15] A. Granados del Águila, E. Groeneveld, J.C. Maan, C. de Mello Donegá, P. C. Christianen, Effect of electron–hole overlap and exchange interaction on exciton radiative lifetimes of CdTe/CdSe heteronanocrystals, *ACS Nano* 10 (4) (2016) 4102–4110.
- [16] S. Brovelli, R.D. Schaller, S.A. Crooker, F. García-Santamaría, Y. Chen, R. Viswanatha, et al., Nano-engineered electron–hole exchange interaction controls exciton dynamics in core–shell semiconductor nanocrystals, *Nat. Commun.* 2 (1) (2011) 1–8.
- [17] X. Yang, A. Wolcott, G. Wang, A. Sobo, R.C. Fitzmorris, F. Qian, et al., Nitrogen-doped ZnO nanowire arrays for photoelectrochemical water splitting, *Nano Lett.* 9 (6) (2009) 2331–2336.
- [18] K. Maeda, T. Takata, M. Hara, N. Saito, Y. Inoue, H. Kobayashi, K. Domen, GaN: ZnO solid solution as a photocatalyst for visible-light-driven overall water splitting, *J. Am. Chem. Soc.* 127 (23) (2005) 8286–8287.
- [19] S.Y. Pung, C.S. Ong, K.M. Isha, M.H. Othman, Synthesis and characterization of Cu-doped ZnO nanorods, *Sains Malaysiana* 43 (2) (2014) 273–281.
- [20] N. Kouklin, Cu-doped ZnO nanowires for efficient and multispectral photodetection applications, *Adv. Mater.* 20 (11) (2008) 2190–2194.
- [21] M. Wang, F. Ren, G. Cai, Y. Liu, S. Shen, L. Guo, Activating ZnO nanorod photoanodes in visible light by Cu ion implantation, *Nano Res.* 7 (3) (2014) 353–364.
- [22] S.M. Lee, S.H. Shin, J. Nah, M.H. Lee, Induced dipole in vanadium-doped zinc oxide nanosheets and its effects on photoelectrochemical water splitting, *Nanotechnology* 28 (39) (2017) 395403.
- [23] L. Cai, F. Ren, M. Wang, G. Cai, Y. Chen, Y. Liu, et al., V ions implanted ZnO nanorod arrays for photoelectrochemical water-splitting under visible light, *Int. J. Hydrogen Energy* 40 (3) (2015) 1394–1401.
- [24] Y. Wang, J. Cheng, S. Yu, E.J. Alcocer, M. Shahid, Z. Wang, W. Pan, Synergistic effect of N-decorated and Mn 2+ doped ZnO nanofibers with enhanced photocatalytic activity, *Sci. Rep.* 6 (2016) 32711.
- [25] P. Giannozzi, S. Baroni, N. Bonini, M. Calandra, R. Car, C. Cavazzoni, et al., QUANTUM ESPRESSO: a modular and open-source software project for quantum simulations of materials, *J. Phys.: Condens. Matter* 21 (39) (2009) 395502.
- [26] J.P. Perdew, K. Burke, M. Ernzerhof, Generalized gradient approximation made simple, *Phys. Rev. Lett.* 77 (18) (1996) 3865.
- [27] D. Vanderbilt, Soft self-consistent pseudopotentials in a generalized eigenvalue formalism, *Phys. Rev. B* 41 (11) (1990) 7892.
- [28] H.J. Monkhorst, J.D. Pack, Special points for Brillouin-zone integrations, *Phys. Rev. B* 13 (12) (1976) 5188.
- [29] L.A. Agapito, S. Curtarolo, M.B. Nardelli, Reformulation of DFT+ U as a pseudohybrid hubbard density functional for accelerated materials discovery, *Phys. Rev. X* 5 (1) (2015), 011006.
- [30] K.K. Korir, A. Catellani, G. Cicero, Ethanol gas sensing mechanism in ZnO nanowires: an ab initio study, *J. Phys. Chem. C* 118 (42) (2014) 24533–24537.

- [31] J. Kaczkowski, A. Jezierski, DFT+ U calculations of transition metal doped AlN, *Acta Phys. Pol. A* 116 (5) (2009) 924–926.
- [32] G. Lan, J. Song, Z. Yang, A linear response approach to determine Hubbard U and its application to evaluate properties of Y₂B₂O₇, B= transition metals 3d, 4d and 5d, *J. Alloys Compd.* 749 (2018) 909–925.
- [33] G. Cicero, A. Ferretti, A. Catellani, Surface-induced polarity inversion in ZnO nanowires, *Phys. Rev. B* 80 (20) (2009) 201304.
- [34] S. Haffad, K.K. Kiprono, Interfacial structure and electronic properties of TiO₂/ZnO/TiO₂ for photocatalytic and photovoltaic applications: a theoretical study, *Surf. Sci.* 686 (2019) 10–16.
- [35] J. Bourgoin, *Point Defects in Semiconductors II: Experimental Aspects*, Vol. 35, Springer Science & Business Media, 2012.
- [36] H. Shi, Y. Duan, First-principles study of magnetic properties of 3 d transition metals doped in ZnO nanowires, *Nanoscale Res. Lett.* 4 (5) (2009) 480.
- [37] H. Ryoken, I. Sakaguchi, N. Ohashi, T. Sekiguchi, S. Hishita, H. Haneda, Non-equilibrium defects in aluminum-doped zinc oxide thin films grown with a pulsed laser deposition method, *J. Mater. Res.* 20 (10) (2005) 2866–2872.
- [38] A. Kudo, Y. Miseki, Heterogeneous photocatalyst materials for water splitting, *Chem. Soc. Rev.* 38 (1) (2009) 253–278.
- [39] K. Ellmer, A. Bikowski, Intrinsic and extrinsic doping of ZnO and ZnO alloys, *J. Phys. D: Appl. Phys.* 49 (41) (2016) 413002.
- [40] P. Singh, R. Kumar, R.K. Singh, Progress on transition metal-doped ZnO nanoparticles and its application, *Ind. Eng. Chem. Res.* 58 (37) (2019) 17130–17163.
- [41] J. Iqbal, T. Jan, Y. Ronghai, S.H. Naqvi, I. Ahmad, Doping induced tailoring in the morphology, band-gap and ferromagnetic properties of biocompatible ZnO nanowires, nanorods and nanoparticles, *Nano-Micro Lett.* 6 (3) (2014) 242–251.
- [42] N. Kamarulzaman, M.F. Kasim, R. Rusdi, Band gap narrowing and widening of ZnO nanostructures and doped materials, *Nanoscale Res. Lett.* 10 (1) (2015) 346.
- [43] J. Iqbal, X. Liu, A. Majid, D. Yu, R. Yu, Narrowing of band gap and low-temperature spin glass behavior of FeNi co-doped ZnO nanowires, *EPL (Europhysics Letters)* 87 (5) (2009) 57004.
- [44] Z. Xu, Q.R. Zheng, G. Su, Charged states and band-gap narrowing in codoped ZnO nanowires for enhanced photoelectrochemical responses: density functional first-principles calculations, *Phys. Rev. B* 85 (7) (2012), 075402.
- [45] R. Vyas, P. Kumar, J. Dwivedi, S. Sharma, S. Khan, R. Divakar, et al., Probing luminescent Fe-doped ZnO nanowires for high-performance oxygen gas sensing application, *RSC Adv.* 4 (98) (2014) 54953–54959.
- [46] Y.K. Hsu, Y.C. Chen, Y.G. Lin, Novel ZnO/Fe₂O₃ core-shell nanowires for photoelectrochemical water splitting, *ACS Appl. Mater. Interfaces* 7 (25) (2015) 14157–14162.
- [47] H.M. Chen, C.K. Chen, Y.C. Chang, C.W. Tsai, R.S. Liu, S.F. Hu, et al., Quantum dot monolayer sensitized ZnO nanowire-array photoelectrodes: true efficiency for water splitting, *Angew. Chem. Int. Ed.* 49 (34) (2010) 5966–5969.
- [48] J. Li, N. Wu, Semiconductor-based photocatalysts and photoelectrochemical cells for solar fuel generation: a review, *Catal. Sci. Technol.* 5 (3) (2015) 1360–1384.
- [49] O.B. Malcıoğlu, R. Gebauer, D. Rocca, S. Baroni, turboTDDFT—A code for the simulation of molecular spectra using the Liouville–Lanczos approach to time-dependent density-functional perturbation theory, *Comput. Phys. Commun.* 182 (8) (2011) 1744–1754.
- [50] Z. Chen, A.Z. Msezane, Effect of C 60 giant resonance on the photoabsorption of encaged atoms, *Phys. Rev. A* 86 (6) (2012), 063405.
- [51] P. Johari, V.B. Shenoy, Tunable dielectric properties of transition metal dichalcogenides, *ACS Nano* 5 (7) (2011) 5903–5908.
- [52] M. Gajdoš, K. Hummer, G. Kresse, J. Furthmüller, F. Bechstedt, Linear optical properties in the projector-augmented wave methodology, *Phys. Rev. B* 73 (4) (2006), 045112.
- [53] P. Liao, E. Carter, New concepts and modeling strategies to design and evaluate photo-electro-catalysts based on transition metal oxides, *Chem. Soc. Rev.* 42 (6) (2013) 2401–2422.
- [54] J. Wang, J. Huang, J. Meng, Q. Li, J. Yang, Enhanced photoelectrochemical performance of anatase TiO₂ for water splitting via surface codoping, *RSC Adv.* 7 (63) (2017) 39877–39884.
- [55] M.M. Obeid, H.R. Jappor, K. Al-Marzoki, I.A. Al-Hydary, S.J. Edrees, M.M. Shukur, Unraveling the effect of Gd doping on the structural, optical, and magnetic properties of ZnO based diluted magnetic semiconductor nanorods, *RSC Adv.* 9 (57) (2019) 33207–33221.
- [56] J. Wang, Y. Huang, J. Guo, J. Zhang, X. Wei, F. Ma, Optoelectronic response and interfacial properties of BiOI/BiOX (X= F, Cl, Br) heterostructures based on DFT investigation, *J. Solid State Chem.* 284 (2020) 121181.
- [57] S.A. Razeq, M.R. Popeil, L. Wangoh, J. Rana, N. Suwandaratne, J.L. Andrews, et al., Designing catalysts for water splitting based on electronic structure considerations, *Electron. Struct.* 2 (2) (2020), 023001.